



HAL
open science

Fundamentals of sol-gel dip-coating

C. Jeffrey Brinker, Alan Hurd

► **To cite this version:**

C. Jeffrey Brinker, Alan Hurd. Fundamentals of sol-gel dip-coating. Journal de Physique III, 1994, 4 (7), pp.1231-1242. 10.1051/jp3:1994198 . jpa-00249179

HAL Id: jpa-00249179

<https://hal.science/jpa-00249179>

Submitted on 4 Feb 2008

HAL is a multi-disciplinary open access archive for the deposit and dissemination of scientific research documents, whether they are published or not. The documents may come from teaching and research institutions in France or abroad, or from public or private research centers.

L'archive ouverte pluridisciplinaire **HAL**, est destinée au dépôt et à la diffusion de documents scientifiques de niveau recherche, publiés ou non, émanant des établissements d'enseignement et de recherche français ou étrangers, des laboratoires publics ou privés.

Classification
Physics Abstracts
81.15

Fundamentals of sol-gel dip-coating

C. Jeffrey Brinker and Alan J. Hurd

Sandia National Laboratories, Advanced Materials Laboratory, 1001 University Blvd, SE ;
Suite 100, Albuquerque, NM 87106, U.S.A.

(Received 23 November 1993, revised 14 March 1994, accepted 29 March 1994)

Résumé. — Pendant l'opération de « dip-coating », le substrat est retiré du sol à vitesse constante. La couche s'amincit du fait de l'évaporation du solvant et de l'écoulement gravitationnel. Après plusieurs secondes, le processus atteint un régime stationnaire. Le profil du film déposé reste alors constant par rapport à la surface du sol. On peut le caractériser *in situ* par des méthodes optiques telles que l'ellipsométrie et la spectroscopie de fluorescence. La texture et les propriétés de la couche dépendent de la taille et de la structure (par exemple de la dimension fractale) des espèces en solution, de l'importance de la tension capillaire pendant le séchage, et des cinétiques de condensation. En contrôlant ces paramètres, on peut faire varier la porosité de la couche dans une large gamme.

Abstract. — During the process of dip-coating, the substrate is withdrawn from the sol at a constant rate. After several seconds, the process becomes steady. The entrained film thins by evaporation of solvent and gravitational draining. Because the shape of the depositing film remains constant with respect to the reservoir surface, it is possible to use analytical methods such as ellipsometry and fluorescence spectroscopy to characterize the depositing film *in situ*. The microstructure and properties of the film depend on the size and structure of the inorganic sol species, the magnitude of the capillary pressure exerted during drying, and the relative rates of condensation and drying. By controlling these parameters, it is possible to vary the porosity of the film over a wide range.

Introduction.

Thin films formed by a dip-coating process represent the oldest commercial application of sol-gel technology. The first patent based on this process was issued to Jenaer Glaswerk Schott & Gen. in 1939 for silica films [1]. Today sol-gel coatings are being studied for a diverse range of applications including protective coatings, passivation layers, ferroelectrics, sensors and membranes [2]. Despite significant advances in technologies based on sol-gel thin-film processing, there has been relatively little effort directed toward understanding the fundamen-

tals of the coating process itself. It is, however, the coating process that serves as the link between the structure of the solution or sol and the microstructure of the deposited film. This paper reviews recent work that addresses the underlying physics and chemistry of sol-gel thin film formation by dip-coating. We first review briefly the aspects of sol-gel chemistry that govern the size and structure of the inorganic species, which along with the solvent(s) comprise the coating sol. We then discuss the salient features of dip-coating based on various means of *in situ* characterization of the film deposition process. Finally, we address the deposition of inorganic sols with regard to time scales and the effects of sol structure and capillary pressure on such properties as refractive index, surface area, and pore size of the deposited film.

Sol-gel chemistry.

The sol-gel process uses inorganic or metal-organic precursors [2]. In aqueous or organic solvents, the precursors are hydrolyzed and condensed to form inorganic polymers composed of M-O-M bonds. For inorganic precursors (salts), hydrolysis proceeds by the removal of a proton from an aquo ion to form a hydroxo (-OH) or oxo (=O) ligand. Condensation reactions involving hydroxo ligands result in the formation of bridging hydroxyl (M- μ (OH)-M) or oxo (M-O-M) bonds. Normally, monomeric aqueous ions are the only stable species at low pH and various monomeric or oligomeric anions the only species observed at high pH. At intermediate pH, well-defined polynuclear ions are often the stable solution species, but the metal solubility is normally limited there and, when exceeded, results in the precipitation of oxyhydroxides or oxides [3].

The most commonly used metal-organic precursors are metal alkoxides, $M(OR)_n$ where R is an alkyl group. Normally the alkoxide is dissolved in its parent alcohol and hydrolyzed by the addition of water plus, in the case of more electronegative metals or metalloids, acid or base catalyst. Hydrolysis replaces alkoxide ligands with hydroxyl ligands. Subsequent condensation reactions involving the hydroxyl ligands produce oligomers or polymers composed of M-O-M or M- μ (OH)-M bonds.

For both inorganic and metal-organic precursors, the structure of the evolving oligomers or polymers depends on the extent of hydrolysis and the preferred coordination number or functionality of the metal [2, 4]. In the case of inorganic precursors, the extent of hydrolysis is generally controlled by the pH, while the effective functionality may be controlled (reduced) through complexation with mono- or multidentate anionic species. The extent of hydrolysis of metal organic precursors is controlled through the hydrolysis ratio H_2O/M and the catalyst concentration. Modification of the alkoxide with chelating or bridging multidentate ligands is generally used to reduce both the effective functionality and the overall extent of condensation [4].

NMR, SAXS, and diffraction studies have documented that the above strategies allow the structure of the condensed species to be varied over a wide range spanning monomers, oligomers, polymers, and nanocrystals [2]. Often so-called « polymeric sols » are characterized by a mass or surface fractal dimension (see following discussion in « Control of Microstructure »).

The only requirements for successful dip-coating are that the condensed phase remain dispersed in the fluid medium, that macroscopic gelation be avoided, and that the sol be sufficiently dilute so that upon deposition the critical cracking thickness not be exceeded (see discussion in « drying stress and cracking »). Thus, in principle, all the above types of sols may be used for dip-coating, although as we shall see, the differences in the structures of the condensed phase lead to differences in the structures of the deposited films.

Dip-coating.

In dip-coating, the substrate is normally withdrawn vertically from the coating bath at a constant speed U_0 (see Fig. 1a) [5]. The moving substrate entrains the liquid in a viscous boundary layer that splits in two at the free surface (point S in Fig. 1b), returning the outer layer to the bath. Since the solvent is evaporating and draining, the entrained film acquires an approximate wedge shape that terminates in a well-defined drying line ($x = 0$ in Fig. 1a). Above the stagnation point S (Fig. 1b), when the upward moving flux is balanced by that due to evaporation, the film position and shape of the film profile remain steady with respect to the coating bath surface. Within the thinning film, the inorganic species are progressively concentrated by evaporation, leading to aggregation, gelation, and final drying to form a type of a dry gel or *xerogel*.

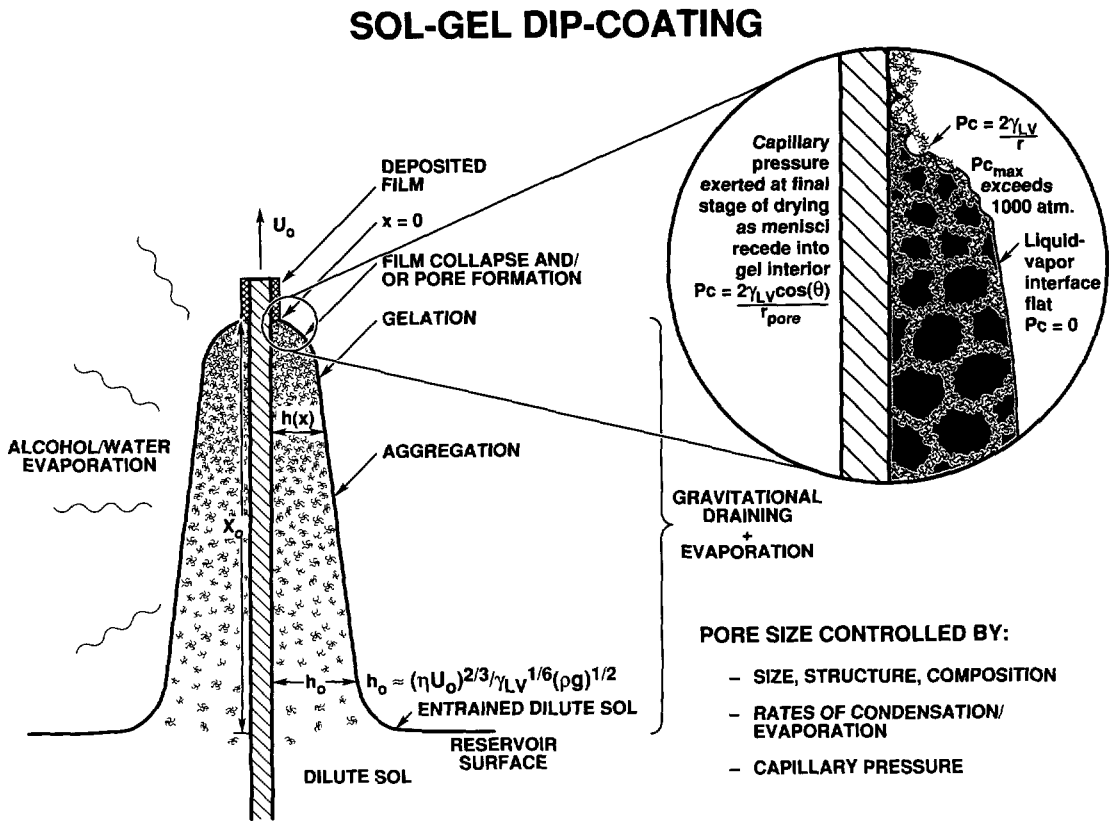


Fig. 1. — a) Schematic of the steady-state dip-coating process, showing the sequential stages of structural development that result from draining accompanied by solvent evaporation and continued condensation reactions, U_0 is the withdrawal speed, $h(x)$ is the film thickness at position x measured from the drying line λ_0 , h_0 is the entrained film thickness just above the stagnation point S, η is the liquid viscosity, ρ is the liquid density, P_c is the capillary pressure, γ_{LV} is the surface tension, and θ is the wetting angle. b) Detail of the flow patterns (streamlines) during dip coating, δ is the boundary layer, and h is the thickness of the fluid film.

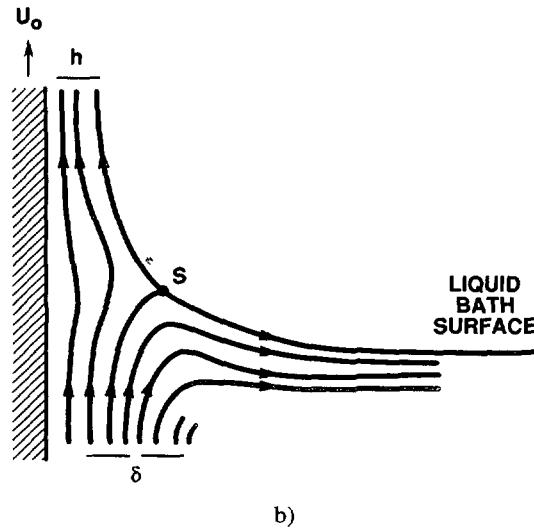


Fig. 1 (continued).

When the substrate speed and liquid viscosity h are low, as is normally the case for sol-gel film deposition, the entrained thickness h_0 (see Fig. 1a) is that which balances the viscous drag ($\propto \eta U_0/h$), gravity force (ρgh), and liquid-vapor surface tension γ_{LV} , according to the relationship derived by Landau and Levich [6] :

$$h_0 = 0.94 (\eta U_0)^{2/3} / \gamma_{LV}^{1/6} (\rho g)^{1/2} \quad (1)$$

where ρ is the liquid density and g is the acceleration of gravity.

Pure and binary fluids.

Although the above expression was developed for pure fluids (i.e. those with no condensed phase), several studies of sol-gel dip-coating have verified the $h \propto U_0^{2/3}$ relationship predicted by equation (1) (e.g., Ref. [7]), suggesting that the entrainment of inorganic species has little effect on the hydrodynamics of dip-coating, at least at the early stages of deposition where the entrained sol is quite dilute. Thus, some insight into sol-gel film deposition may be gained by closer examination of the details of gravitational draining and evaporation of pure and binary fluids as revealed by « imaging ellipsometry » [8] and « fluorescence imaging » [9] of the steady state film profile (see Fig. 2). Imaging ellipsometry allows the *in situ* determination of film thickness h and film refractive index n over the complete film profile depicted in figure 1a. Fluorescence imaging, figure 2, uses entrained organic dyes as molecular sensors of the progressively changing physical and chemical environments created within the thinning film.

Whereas the entrained film thickness immediately above the stagnation point depends on hydrodynamic factors, the shape of the film profile $h(x)$ in the vicinity of the drying line is established by the evaporation rate. Hurd showed that for planar substrate geometry, the evaporation rate E of a pure fluid was not constant but diverged at the drying line ($x = 0$, Fig. 1a) according to the expression [10] :

$$E(x) = -D_v a x^{-1/2} \quad (2)$$

ORGANIC OPTICAL MOLECULAR SENSORS OF FILM DEPOSITION

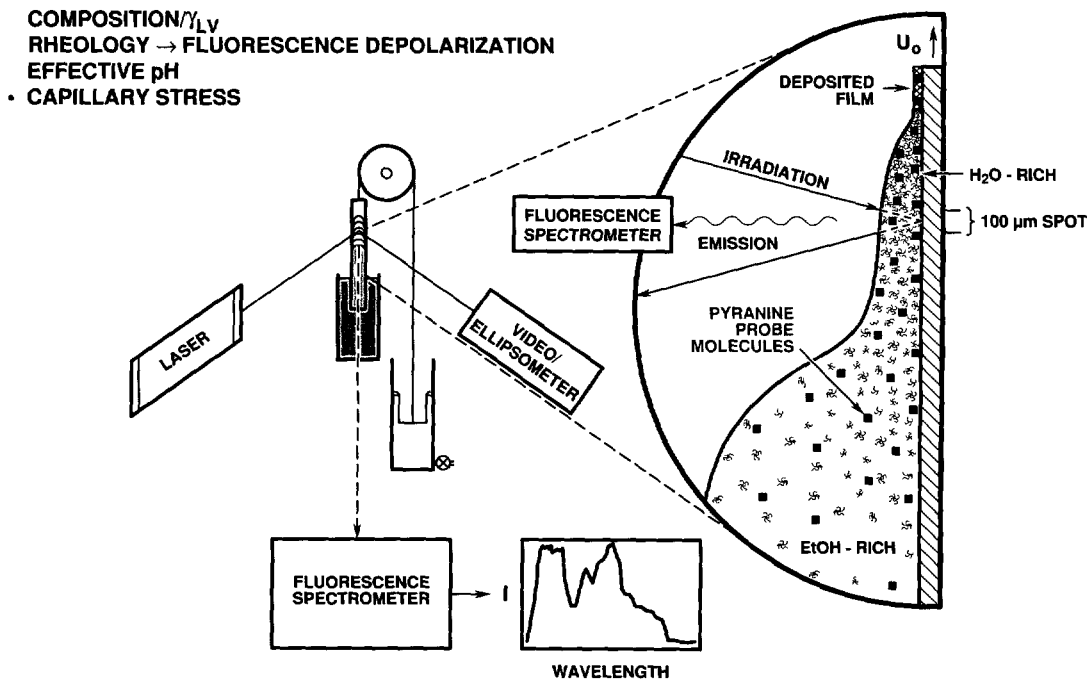


Fig. 2. — Schematic of fluorescence imaging apparatus. Organic optical molecules are entrained in the depositing film. Spatially resolved fluorescence spectroscopy provides information concerning the local environments of the probe molecules as they are transported from the dilute sol to the deposited film.

where D_v is the diffusion coefficient of the vapor, and a is a constant. The divergence of the evaporation rate causes the film to thin more quickly in the vicinity of the drying line, so instead of exhibiting a wedge-shape (the expectation for uniform evaporation) the film profile acquires a parabolic shape :

$$h(x) \sim \int E(\lambda) dx \sim x^{1/2} \quad (3)$$

For multicomponent fluids (e.g., alcohol/water mixtures often used in alkoxide-based sols) differences in the evaporation rates and surface tensions of the individual fluid components alter the shape of the film profile and create convective flows within the depositing film. For example, for binary alcohol/water mixtures, the film profile shows two roughly parabolic regions (see Fig. 2). The first corresponds to the preferential evaporation of alcohol to leave a water-rich fluid. The difference in surface tensions between the water-rich and alcohol-rich regions induces liquid flow into the water-rich « foot » with velocity u the so-called « Marangoni effect » [5, 7] :

$$u = 1/\eta [d\gamma/dx] z - U_0 \quad (4)$$

where z is the direction normal to the substrate surface. The foot slowly grows until this flux is balanced by that of evaporation from the expanding free surface.

There are several consequences of preferential evaporation and surface tension gradient driven flows with respect to sol-gel film deposition :

i) it is the composition of the fluid that persists to the drying line that establishes the surface tension and hence the magnitude of the capillary pressure exerted on the condensed phase (Fig. 1a). Fluorescence imaging (Fig. 2) performed by Nishida and co-workers [9] has shown that for ethanol/water/silica sols, the composition of the fluid at $x = 0$ is greater than 80 % water, when the initial sol contains only 12.5 volume % water ;

ii) the surface tension gradient-driven flow of liquid through a thin « neck » can create quite high shear rates during dip-coating. For the toluene:methanol (50:50) system, the shear rate resulting from surface tension gradient driven flow is estimated to be 10^4 s^{-1} [10]. Such shears could be sufficiently strong to align or order the entrained inorganic species.

Effect of condensed phases.

SOLIDS CONCENTRATION AND TIME SCALE. — As the film thins, the entrained condensed species are concentrated. Above the stagnation point where all entrained species are incorporated in the final deposited film, a simple flux balance over a horizontal slice leads to [10] :

$$h(x) \phi(x) = \text{Cte} + \vartheta (h^2/h_0^2) \quad (5)$$

where $\phi(x)$ is the volume fraction solids. We see that ϕ varies inversely with h , if $h \ll h_0$ (the normal case for sol-gel dip-coating). This rapid concentration is more evident from consideration of the mean particle (polymer) separation distance $\langle r \rangle$, which varies as the inverse cube root of ϕ , or $\langle r \rangle \sim \phi^{-1/3}$. This precipitous function implies that half the distance between particle (polymer) neighbors is traveled in the last 2 % of the deposition process, establishing a time scale of about 0.1 s during which the condensed species are in close proximity.

We anticipate several consequences of the short time scale of the film deposition processes. i) There is little time available for reacting species to « find » low energy configurations. Thus (for reactive systems) the dominant aggregative process responsible for network formation may change from reaction-limited (near the reservoir surface) to transport-limited near the drying line. ii) For sols composed of repulsive particles, there is little time available for the particles to order as they are concentrated in the thinning film. iii) There is little time available for condensation reactions to occur. Thus gelation may actually occur by a physical process, through the concentration dependence of the viscosity rather than a chemical process. (In some systems this is evident by the fact that the deposited film is quickly re-solubilized when immersed in solvent [11]). iv) Since the thin physical or chemical gels are likely more weakly condensed, and hence, more compliant than bulk gels, they are more easily compacted ; first by evaporation and then by the capillary pressure exerted at the final stage of the deposition process (see Fig. 1a). In such compliant materials the effects of capillary forces are enhanced, because greater shrinkage precedes the critical point, where the liquid-vapor interface first recedes into the gel (Fig. 1a inset), causing the pore size to be smaller and the maximum capillary pressure to be greater (see following discussion of drying).

STAGES OF DRYING. — Scherer [12] divides the drying of gels into two stages : a constant rate period (CRP) and a falling rate period. During the constant rate period, mass transfer is limited by convection away from the gel surface, whereas during the falling rate period, mass transfer is limited by the permeability of the gel. Extending these ideas to dip-coating, we might expect that a CRP would obtain throughout most of the deposition process, since the liquid-vapor

interface remains located at the exterior surface of the thinning film except at the final stage of drying (see Fig. 1a).

A constant evaporation rate implies a wedge-shaped film profile. This is not observed for pure fluids, nor is it observed for inorganic sols. The film profile of a titanate sol prepared from titanium ethoxide hydrolyzed under acidic conditions in ethanol is described by $h(x) \sim x^{0.62}$ [5], which indicates that the evaporation rate increases as $x \rightarrow 0$, although not quite as rapidly as for pure ethanol ($h(x) \sim x^{0.5}$). Thus even for the deposition of inorganic sols, the film profile, and hence the concentration profile, are largely established by the dependence of the evaporation rate on the geometry of the depositing film⁽¹⁾. For sols containing fluid mixtures of differing volatilities, the fluid composition changes with distance x , contributing to further changes in the evaporation rate.

The critical point, where the liquid first recedes into the gel (see Fig. 1a inset) should mark the beginning of the falling rate period. Depending on the distribution of liquid in the pores, the drying rate is limited by flow or diffusion. For compliant molecular networks that are collapsed prior to the critical point, drying occurs by Fickian diffusion, if the temperature is above the glass transition temperature of the mixture [12]. The onset of a falling rate period near the drying line may account for the differences in the exponents that describe the shape of the pure fluid and the titanate sol film profiles.

RHEOLOGY. — As the film becomes more concentrated in the condensed phase through evaporation, the rheological response of the liquid changes from Newtonian to shear thinning (aggregated systems) or thixotropic (ordered systems) and then to viscoelastic. Eventually gelation extends throughout the film and the material no longer yields; i.e. the film behaves as an elastic solid. It is at this final stage of the deposition process that the capillary pressure P_c created by tiny menisci as they recede into the gel, is maximized (see Fig. 1a). The curvature of the menisci causes the liquid to be in tension and the network in compression. Generally the magnitude of the capillary pressure is estimated by the Laplace equation :

$$P_c = -2 \gamma_{LV} \cos(\theta) / r_p \quad (6)$$

where θ is the wetting angle and r_p is the pore size. For wetting pore fluids ($\cos \theta \rightarrow 1$), P_c could approach or possibly exceed 1 000 bar, because the pore size may approach molecular dimensions. The capillary pressure thus represents a very strong driving force to densify the depositing film.

It is balance between this capillary pressure, which compresses the network, and the modulus of the network, which enables it to resist collapse, that establishes the final density and pore size of the film. Initially as the solvent evaporates, the gel is able to shrink. The volume fraction solids ϕ increases, causing the bulk modulus K to increase as a power law. For both wet and dry silica gels, the following relationship is observed [12] :

$$K \propto \phi^{3.8} \quad (7)$$

At the same time the spacing between polymers (effective pore size) is decreasing, causing the maximum possible capillary pressure to increase approximately as $1/\langle r \rangle \sim \phi^{1/3}$. Thus for silica films, we expect the modulus to increase more rapidly than the capillary pressure. When the modulus rises sufficiently to balance the capillary pressure, shrinkage stops, thereby

⁽¹⁾ Experiments performed on a variety of substrates, including metals, ceramics, and plastics all showed similar thickness profiles emphasizing that the evaporation rate not the wetting characteristics are responsible for determining the profile shape [10].

establishing the pore size and density. Beyond this so-called critical point any further solvent loss creates porosity within the film. For systems in which K exhibits a much weaker dependence on ϕ , for example as a consequence of organic modification or complexation of the metal centers with multidentate, non-hydrolyzable ligands, we might expect the network to be completely collapsed by the rising capillary pressure. However the rising viscosity accompanying solvent loss combined with the short time scale of the deposition process may represent a kinetic limitation to achieving a non-porous state. (It should also be pointed out that subsequent thermolysis of organic ligands will normally create porosity, even though the as-deposited film could be considered non-porous).

Drying stress and cracking.

As the film dries, it shrinks in volume. Once the film is attached to the substrate and unable to shrink in that direction, the reduction in volume is accommodated completely by a reduction in thickness. When the film has solidified and stresses can no longer be relieved by flow, tensile stresses develop in the plane of the substrate. Croll [13] estimated the stress (σ) as :

$$s = [E/(1 - \nu)][(f_s - f_r)/3] \quad (8)$$

where E is Young's modulus (Pa), ν is Poisson's ratio, f_s is the volume fraction solvent at the solidification point, and f_r is the volume fraction of residual solvent in the « dry » film. The solidification point was defined for a polymer film as the concentration where the glass transition temperature has risen to the experimental temperature. Thus stress is proportional to Young's modulus and the difference between the solvent fraction at the solidification point and that of the dried coating. Scherer [2, 12] states that the stress in the film is very nearly equal to the tension in the liquid ($\sigma \approx P_c$). Despite such a large stress, it is commonly observed that cracking of films does not occur if the film thickness is below a certain critical thickness $h_c \cong 0.5\text{-}1 \mu\text{m}$ [12]. For films that adhere well to the substrate, the critical thickness for crack propagation or the growth of pinholes is given by [14, 15] :

$$h_c = (K_{Ic}/\sigma \Omega)^2 \quad (9)$$

where K_{Ic} is the critical stress intensity or « fracture toughness » and Ω is a function that depends on the ratio of the elastic modulus of the film and substrate (for gel films $\Omega \cong 1$). For films thinner than h_c , the energy required to extend the crack is greater than the energy gained from relief of stresses near the crack, so cracking is not observed [12].

When the film thickness exceeds h_c , cracking occurs, and the crack patterns observed experimentally are qualitatively consistent with fractal patterns predicted by computer simulation [16]. Atkinson and Guppy [17] observed that the crack spacing increased with film thickness and attributed this behavior to a mechanism in which partial delamination accompanies crack propagation. Such delamination was observed directly by Garino [18] during the cracking of sol-gel silicate films.

Based on equations (8) and (9) above, strategies to avoid cracking include : i) increasing the fracture toughness (K_{Ic}) of the film, ii) reducing the modulus of the film, iii) reducing the volume fraction of solvent at the solidification point, and iv) reducing the film thickness. In organic polymer films, plasticizers are often added to reduce the stiffness of the film and thus avoid cracking [19]. For sol-gel systems, analogous results are obtained by organic modification of alkoxide precursors [20], chelation by multidentate ligands such as β -diketonates [21] or a reduction in the extent of hydrolysis of alkoxide precursors [18].

It should be noted that for particulate films Garino [22] observed that the maximum film thickness obtainable without cracks decreased linearly with a reduction in particle size. Since

for unaggregated particulate films, the pore size scales with the particle size, this effect may be due to an increase in the stress caused by the capillary pressure ($\sigma \cong P_c$) and/or an increase in the volume fraction solvent at the solidification point resulting from the manner that the electrostatic double layer thickness (estimated by the Debye-Huckel screening length) varies with particle size [23].

Control of microstructure.

The final film microstructure depends on : i) the structure of the entrained inorganic species in the original sol (for example, size and fractal dimension), ii) the reactivity of these species (for example, condensation or aggregation rates), iii) the time scale of the deposition process (related to evaporation rate and film thickness), and iv) the magnitude of shear forces and capillary forces that accompany film deposition (related to surface tension of the solvent or carrier and surface tension gradients). The most common means of controlling the film microstructure is through particle size. For unaggregated, monosized particulate sols, the pore size decreases and the surface area increases with decreasing particle size. Asymmetric, supported membranes have been prepared successfully from particulate sols for use in ultrafiltration [24]. As noted above difficulties arise when trying to prepare microporous membranes due to an increased tendency for cracking. Particulate sols may be intentionally aggregated prior to film formation to create very porous films [25] (e.g., volume porosity > 65 %). For electrostatically stabilized silica sols, a transition from random-close packing to ordered packing is observed with increasing substrate withdrawal rates (U_0) [25]. This may be due to a longer time scale of the deposition process (providing more time for ordering) or an increase in the shear rate accompanying deposition for higher U_0 [25].

A second strategy [2] for controlling porosity is based on the scaling of mass M_f and size r_f of a mass fractal object :

$$M_f \sim r_f^D \quad (10)$$

where D is the mass fractal dimension (in three dimensional space, $0 < D < 3$). Since density equals mass/volume, the density ρ_f of a mass fractal object varies in three dimensional space as $\rho_f \sim r_f^D/r_f^3$, and the porosity varies as $1/\rho_f \sim r_f^{(3-D)}$. Thus the porosity of a mass fractal object increases with its size. Providing that such fractals do not completely interpenetrate during film formation (i.e., they are mutually opaque, requiring $D > 1.5$ [2]), the porosity may be controlled by the size of the entrained fractal species prior to film formation. The efficacy of this approach is illustrated in [Ref. [25]] where the refractive index, volume fraction porosity, pore size, and surface area of a multicomponent silicate film were shown to vary monotonically with aging time employed to grow the fractal species prior to film deposition. The extent of interpenetration of colliding fractals depends on their respective mass fractal dimensions and the condensation rate or « sticking probability » at points of intersection. A reduction of either D or the condensation rate increases the interpenetration and decreases the porosity [2, 25]. From equation (10) and surrounding discussion, it follows that to generate porosity using this fractal scheme, r_f should be rather large, $1.5 \ll D \ll 3$, and the condensation rate should be high. Conversely dense films should be formed from small, unreactive precursors consistent with observations made on a variety of films prepared from chelated single and multicomponent alkoxide precursors [11].

The magnitude of the capillary pressure P_c should also be quite influential in determining microstructure. For bulk gels, elimination of surface tension by removal of the pore fluid above its critical point [26] results in highly porous aerogels. Deshpande and co-workers have recently shown that, for aprotic pore fluids, the surface area, pore volume, and pore size of

bulk silica xerogels are all reduced monotonically by an increase in surface tension of the pore fluid [27]. Such studies are more difficult for films, since it is not possible to wash the coating sol, and distillation of solvents often leads to premature gelation. The most revealing studies are those comparing the effects of different hydrolysis ratios, $H_2O/M(OR)_n$, on film properties. Since the theoretical ratio for complete hydrolysis and condensation is $n/2$, greater ratios must produce « excess » water. As described above in mixed solvent systems, the least volatile component survives to the drying line and therefore dictates the magnitude of the capillary pressure.

Fluorescence imaging experiments have shown that for alcohol/water mixtures containing more than about 10 volume % water, the composition of the fluid at the drying line is 100 % water [9]. We have shown that as the « excess » water is increased from 0.5 to 6.0 volume %, the refractive index of silica films deposited by dipping increases from 1.342 to 1.431, corresponding to a reduction in porosity from 22 % to 7 % [28]. Further increases in the excess water content cause a reduction in refractive index (increase in porosity). Since water increases both the surface tension and the extent of condensation of the silicate matrix, this behavior reflects the competition between capillary pressure, which compacts the film, and aging, which stiffens the film increasing its resistance to compaction. In a similar dip-coating study, Warren and coworkers [29] observed that, for silica films annealed at 800 °C, the dielectric strength increased and the HF etch rate decreased as the hydrolysis ratio of the coating sol increased from 1 to 7.5. Further increases caused the reverse behavior. This implies that the effects of capillarity and aging also strongly influence the subsequent consolidation process.

Finally it is anticipated that shear forces accompanying film formation could influence microstructure. Although the withdrawal rates U_0 are often very low in dip-coating, we have shown that surface tension gradient driven flows can cause high shear rates (10^4 s^{-1}) near the drying line [28]. Such shear rates might be partially responsible for the ordering of monosized particulate films [28]. Spin-coating is characterized by higher shear rates. Several studies have shown that the refractive index increases or decreases with increasing rotational speed [2, 30]. Presumably these conflicting results are explained by the effects of both time scale and shear on microstructural development : increasing the rotational speed increases the shear rate and reduces the characteristic time scale.

Summary.

It is the sol-gel dip-coating process that serves as the link between the structure and properties of the liquid precursor sol and the microstructure of the corresponding deposited film. The steady film profile depicted in figure 1 spatially resolves the complete sol to gel to xerogel transformation. Spatially resolved *in situ* characterization of this deposition process, using imaging ellipsometry and fluorescence imaging, allows us to gain a fundamental understanding of the physics and chemistry of sol-gel film deposition as well as to provide insight into sol-gel processing in general.

Acknowledgements.

This work was supported by the U.S. Department of Energy Basic Energy Sciences Program. This work was performed at Sandia National Laboratories, a U.S. Department of Energy Laboratory, under contract number DE-AC04-94AL85000.

References

- [1] Geffcken W. and Berger E., Deutsches Reichspatent 736411, May 6, 1939, assigned to Jenaer Glaswerk Schott & Gen., Jena.
- [2] Brinker C. J. and Scherer G. W., Sol-Gel Science (San Diego, Academic Press, 1990).
- [3] Baes C. F. and Mesmer R. E., The Hydrolysis of Cations (New York, Wiley, 1976).
- [4] Livage J., Henry M. and Sanchez C., Sol-Gel Chemistry of Transition Metal Oxides, *Prog. Solid St. Chem.* **18** (1988) 259-342.
- [5] Brinker C. J., Hurd A. J., Frye G. C., Schunk P. R. and Ashley C. S., Sol-Gel Thin film Formation, *J. Ceram. Soc. Jpn* **99** (1991) 862-877.
- [6] Landau L. D. and Levich V. G., Dragging of a liquid by a moving plate, *Acta Phys. Chim. URSS* **17** (1942) 42-54.
- [7] Brinker C. J., Hurd A. J., Schunk P. R. and Ashley C. S., Review of Sol-Gel Thin Film Formation, *J. Non-Cryst. Solids* **147 & 148** (1992) 424-436.
- [8] Hurd A. J. and Brinker C. J., Optical Sol-Gel Coatings : Ellipsometry of Film formation, *J. Phys. France* **49** (1988) 1017-1025.
- [9] Nishida F., Dunn B., Mckiernan J. M., Zink J. I., Hurd A. J. and Brinker C. J., *in situ* Fluorescence Imaging of Sol-Gel Thin Film Formation ; Proceedings of VIIth Intl. Workshop on Glasses and Ceramics From Gels, July 19-23, 1993, Paris, France to be published (1993).
- [10] Hurd A. J., Evaporation and surface tension effects in dip coating, *Adv. Chem. Series No. 234*, Am. Chem. Soc., to be published January (1994).
- [11] Schwartz R. W., Voigt J. A., Buchheit C. D. and Boyle T. J., Densification and crystallization of zirconia thin films prepared by sol-gel processing, Ceramic Transactions-Proc. Am. Ceram. Soc. PAC RIM Mtg., Honolulu, HI (November, 1993) submitted.
- [12] Scherer G. W., Recent Progress in Drying of Gels, *J. Non-Cryst. Solids* **147 & 148** (1992) 363-374.
- [13] Croll S. G., The Origin of Residual Internal Stress in Solvent-Cast Thermoplastic Coatings, *J. Appl. Polymer Sci.* **23** (1979) 847-853.
- [14] Evans A. J., Dory M. D. and Hu M. S., The Cracking and Decohesion of Thin Films, *J. Mats. Res.* **3** (1988) 1043-1054.
- [15] Thouless M. D., Decohesion of Films with Axisymmetric Geometrics, *Acta Metall.* **36** (1988) 3131-3139.
- [16] Meakin P., Models for Materials Failure and Deformation, *Science* **252** (1991) 226-229.
- [17] Atkinson A. and Guppy R. M., Mechanical Stability of Sol-Gel Films, *J. Mater. Sci.* **26** (1991) 3869-3875.
- [18] Garino T. J., The Cracking of Sol-Gel thin films During Drying in Better Ceramics Through Chemistry IV, **180** (1990) 497-502, MRS.
- [19] Cohen E. D., Gutoff E. B. and Lightfoot E. J., in Proc. 1990 Int. Symp. on Mechanics of Thin Film Coating, AIChE Spring Mtg. Orlando FL (March 1990).
- [20] Schmidt H., Rinn G., Nass R. and Sporn D., Film Formation by Inorganic-Organic Sol-Gel Synthesis, in Better Ceramics through Chemistry III **121** (1988) 743-752, MRS.
- [21] Takahashi Y., Matsuoka Y., Yamaguchi Kouichi, Matsuki M. and Kobayashi K., Dip coating of PT, PZ, and PZT films using an alkoxide-diethanolamine method, *J. Mater. Sci.* **25** (1990) 3960-3964.
- [22] Garino T. J., PhD Thesis, MIT (1988).
- [23] Brinker C. J. and Scherer G. W., Sol-Gel Science chap. 4 (Academic Press, San Diego, 1990) pp. 235-301.
- [24] Many examples are provided in R. R. Bhave, Ed., Inorganic Membranes (Van Nostrand Reinhold, New York, 1991).
- [25] Brinker C. J., Hurd A. J., Frye G. C., Ward K. J. and Ashley C. S., Sol-Gel Thin Film Formation, *J. Non-Cryst. solids* **121** (1990) 294-308.
- [26] Brinker C. J. and Scherer G. W., Sol-Gel Science chap. 8 (Academic Press, San Diego, 1990) pp. 493-505.

- [27] Deshpande R., Hua D.-W., Smith D. M. and Brinker C. J., Pore Structure Evolution in Silica Gels during Aging and Drying : 3. Effects of Surface Tension, *J. Non-Cryst. Solids* **144** (1992) 32-43.
- [28] Brinker C. J., Frye G. C., Hurd A. J. and Ashley C. S., Fundamentals of Sol-Gel Dip Coating, *Thin Solid Films* **201** (1991) 97-108.
- [29] Warren W. L., Lenahan P. M., Brinker C. J., Shaffer G. R., Ashley C. S. and Reed S. T., Sol-Gel Thin Film Electronic Properties, in *Better Ceramics Through Chemistry IV* **180** (1990) 413-419, MRS.
- [30] Glaser P. M. and Pantano C. G., Effect of the H₂O/TEOS ratio upon the preparation and nitridation of silica sol/gel films, *J. Non-Cryst. Solids* **63** (1984) 209-215.